TiO2nanotubes in lithium-ion batteries

TiO_2 nanotubes in lithium-ion batteries

Cite as: AIP Conference Proceedings **2257**, 020006 (2020); https://doi.org/10.1063/5.0023681
Published Online: 03 September 2020

Antonio Rubino, Marco Agostini, Pier Giorgio Schiavi, Pietro Altimari, and Francesca Pagnanelli

TiO_2 Nanotubes in Lithium-Ion Batteries

Antonio Rubino[1, a)], Marco Agostini[2], Pier Giorgio Schiavi[1], Pietro Altimari[1] and Francesca Pagnanelli[1]

[1]*Department of Chemistry, Sapienza University of Rome, P.le Aldo Moro 5, 00185, Rome, Italy*
[2]*Department of Applied Physics, Chalmers University of Technology, S41296, Gothenburg, Sweden*

[a)] Corresponding author: antonio.rubino@uniroma1.it

Abstract. In this contribution we report on electrochemical approaches in TiO_2 based electrodes synthesis. TiO_2 nanotubes (NTs) were synthesized following a facile anodization of titanium sheets. Optimizing the experimental conditions two electrodes with NTs lengths of ~ 10 µm (Long) and ~ 2 µm (Short), were obtained. At the end of the anodization the amorphous TiO_2 (a-TiO_2) was thermally treated to promote the conversion in the anatase crystal phase (c-TiO_2). Both the Long and Short NTs electrodes were tested for their applications as anodes in lithium-ion batteries (LIBs). A preliminary comparison was performed to evaluate the role of a-TiO_2 and c-TiO_2 phases. Here, Short a-TiO_2 NTs exhibited a fast storage rate respect to Short c-TiO_2. Comparing the NTs length, Long a-TiO_2 electrodes exhibited the highest specific capacity, close to the theoretical value. Furthermore, all the electrodes tested showed an excellent capacity retention proceeding with Discharge/Charge cycles.

INTRODUCTION

In the last decades TiO_2 has been object of study and claimed as one of the most promising electrodic materials in Lithium-ion batteries (LIBs), specifically in reason of its chemical stability, non-toxicity, availability and low cost [1]. In its crystal phase Anatase, it would be characterized by fast Li^+ storage rate and high theoretical insertion capacity [2,3]. At the same time, amorphous TiO_2, thanks to its disordered structure, would provide intercalation pseudocapacitive contributions to the overall capacity, achieving better electrochemical performances especially at higher charge/discharge rate [4].

TiO_2 nanotubes (NTs) supported over titanium sheets can be synthesized through potentiostatic anodization of titanium substrate, offering a low cost and versatile nanofabrication method [5–7]. Specifically, tuning experimental parameters like cell voltage, pH, electrolyte composition and time of the electrolysis, is possible to determine characteristics as NTs diameter and length [6,8–12].

The resulting highly ordered and vertically oriented TiO_2 NTs, in reason of the ordered material architecture, are excellent electron percolation pathways for vectorial charge transfer across interfaces [13]. These characteristic confers outstanding charge transport and carrier lifetime properties which makes this material particularly appealing in advanced energy storage applications as LIBs [14].

The most diffused anodization methods are based on “double step” processes, consisting of two anodizations separated by the selective removal of the first-formed oxide [15,16]. Some Authors report on ordered NTs achieved by single-step anodization methods, namely with two operation less than conventional double-steps [17,18]. It is carried out controlling the cell voltage in the early stage of the process, prior to proceed with the potentiostatic anodization [7,19].

Here, major obstacle to produce considerably short nanotubes is the formation of a disordered layer (overlaying NTs) during the early stage of the anodization. This layer is characterized by a large polydispersity of the diameter distribution [19], which would affect negatively the charge transfer at the electrode/electrolyte interface.

NANOINNOVATION 2019
AIP Conf. Proc. 2257, 020006-1–020006-8; https://doi.org/10.1063/5.0023681
Published by AIP Publishing. 978-0-7354-2017-5/$30.00

Based on that, aim of the present study has been the optimization of the anodization to achieve electrodes with different lengths of the NTs layer, prior to evaluate their effect on the performances of the assembled Lithium-ion cells.

MATERIALS AND METHODS

TiO_2 NTs Based Electrodes Synthesis

TiO_2 NTs based electrodes were produced by a single-step anodization method developed in our previous report [19]. Briefly, titanium planar electrodes (Alfa Aesar 99.5%, annealed, thickness 0.25mm) have been employed in a symmetric cell scheme (i.e. same electrodes for anode and cathode), kept at room temperature and magnetically stirred. The electrolyte was Ethylene Glycol (Alfa Aesar, 99+%) based, containing 0.3 %wt NH_4F (Alfa Aesar, 98% min.) and 1.0 %v/v pure H_2O. The anodization process started with a linear increase (0.5 V s^{-1}) of the cell voltage up to 60 V. Afterwards, the anodization voltage was kept constant for 60 minutes. The synthesis included a sonication post-treatment after the anodization.

Based on this method an optimization has been proposed. It consists of the adjustment of the NH_4F/H_2O ratio in the Ethylene Glycol based electrolyte and the tuning of the cell voltage growth rate in the early stage of the process, as summarized in Table 1 (AM2-AM6).

The conversion of the amorphous titania (a-TiO_2) resulting from the anodization in its crystal anatase phase (c-TiO_2) was promoted through a thermal treatment in a muffle furnace (Nabertherm B410, Tmax1100°C, 1.2KW) at 580 °C for 132.5 minutes. Treatment temperature was reached with heating rate of 8 °C min^{-1}.

TABLE 1. Experimental conditions of the anodization processes tested.

Method	NH_4F [%wt]	H_2O [%v/v]	Voltage rate [V s^{-1}]	Voltage [V]	Anodization time [min]
AM1	0.3	1.0	0.5	60	62
AM2	0.3	1.0	0.5	60	17
AM3	0.3	10.0	0.5	60	17
AM4	0.3	15.0	0.5	60	17
AM5	0.3	6.0	0.5	60	9
AM6	0.3	6.0	0.05	60	27

Electrodes Characterization

The synthesized electrodes have been analyzed through a field emission scanning electron microscopy (FE-SEM Zeiss Auriga), to characterize morphology and dimensions of the nanostructures. The software ImageJ was used to analyze FE-SEM images.

The phase composition of the NTs was determined through an X-ray diffractometer (Bruker D8 ADVANCE) with a Molybdenum anode (Kα1 = 0.709319Å). It has been employed for the characterization of the Ti sheets prior to be anodized, and Ti/TiO_2 electrodes before (a-TiO_2) and after (c-TiO_2) the annealing treatment.

Electrochemical Tests

Electrodes listed in Tab.2 were alternatively employed as anodes in Swagelok-type cells for the Li^+ insertion/extraction properties study. The assembled cells include a Celgard 2400 (12 mm; 1.2 mg cm^{-2}) separator soaked with 10 µL cm^{-2} of DOL:DME (1:1 w:w), $LiNO_3$ 0.8 M/LiTFSI 1.0 M electrolyte, and a lithium disk (11 mm, 4 mg cm^{-2}). The TiO_2 based electrodes active surface was 1 cm^2 in each test.

The lithium-ion extraction/insertion properties have been evaluated by galvanostatic charge/discharge tests in the potential range within 1.0 and 2.5 V, at 100, 300, 500, 800 and 1000 mA g^{-1} current densities, for all the electrodes tested.

The specific capacity of the Li half-cells has been estimated considering only the weight of the TiO_2 NTs layer supported over the Ti current collector. The specific weight of the TiO_2 layer (Tab.2) in the different electrodes, was approximately estimated through the geometrical characteristics derived from the FE-SEM images analysis.

TABLE 2. Electrodes tested in Swagelok-type cells.

NTs type	TiO_2 phase	Specific weight [g cm^{-2}]
Long	Amorphous	0.00210
Long	Anatase	0.00190
Short	Amorphous	0.00053
Short	Anatase	0.00047

RESULTS AND DISCUSSION

Short NTs Synthesis. Optimization of the Anodization Parameters

Long NTs, characterized by ~10 μm length, have been synthesized through the anodization method AM1 (Tab.1). The synthesis included a sonication post-treatment for the removal of an undesired nano-grass layer, generated proceeding with the anodization time as a consequence of the electrolyte etching effect on the early formed oxide (i.e. top of the tubes) [19]. Figure 1-A shows the relative FE-SEM images, highlighting the nano-grass free morphology (Fig.1-A, insert).

According to the same method, reducing the anodization time reduced NTs lengths (i.e. TiO_2 layer thickness) would be achieved.

In Fig.1-B are shown FE-SEM images related to NTs synthesized in the same experimental conditions mentioned above but reducing the anodization time to 17 minutes (Tab.1, AM2).

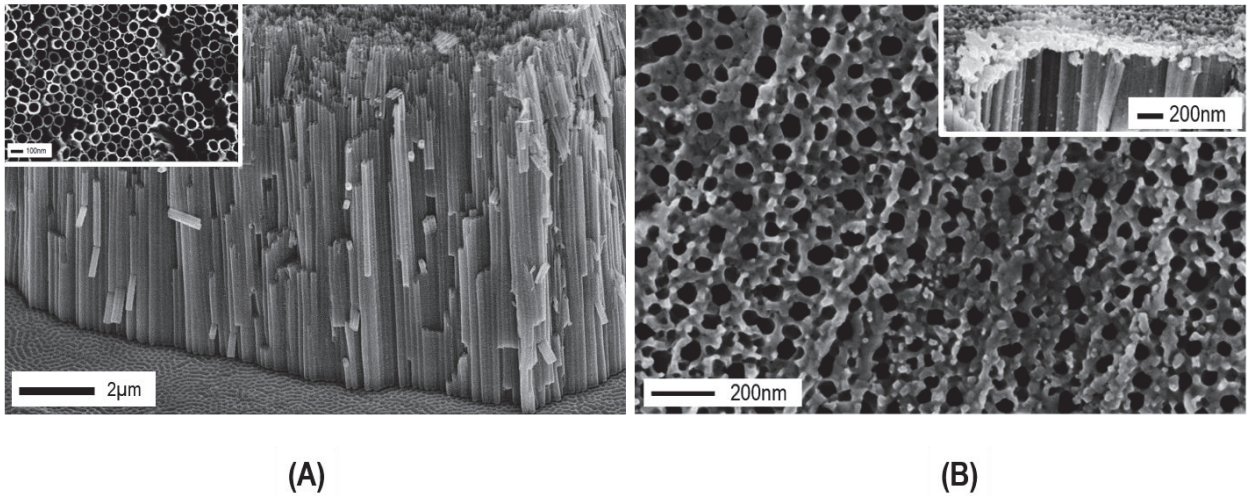

FIGURE 1. FE-SEM images. A) Cross sectional view of Long NTs achieved through AM1 (Tab.1) after sonication treatment. The insert (on top left) is the top view. B) Top view of TiO_2 NTs achieved based through AM2 (Tab.1). The insert (on top right) is the correspondent cross sectional view.

As highlighted in the insert of Fig.1-B, a disordered layer (tree-like layer), characterized by a high heterogeneity in the inner tube diameters, hang over the NTs array. This undesired morphology is due to the potentiodynamic behavior of the cell voltage in the early stage of the process. It disappears as effect of the electrolyte etching for longer anodization times, which inevitably increase the overall NTs length.

To overcome this limit an optimization of the anodization parameters has been proposed. It has been performed investigating both, different NH_4F/H_2O concentration ratios (Tab.1, AM3-AM5) and further adjusting the voltage growth rate in the early stage of the anodization (Tab.1, AM6).

Figure 2 shows the TiO_2 NTs synthesized increasing the water content to 6.0 %v/v and decreasing the voltage growth rate to 0.05 V s^{-1} (Tab.1, AM6). This anodization method allowed to achieve ordered Short NTs, characterized by a NTs length ≤ 2 μm and inner diameters ≥ 50 nm.

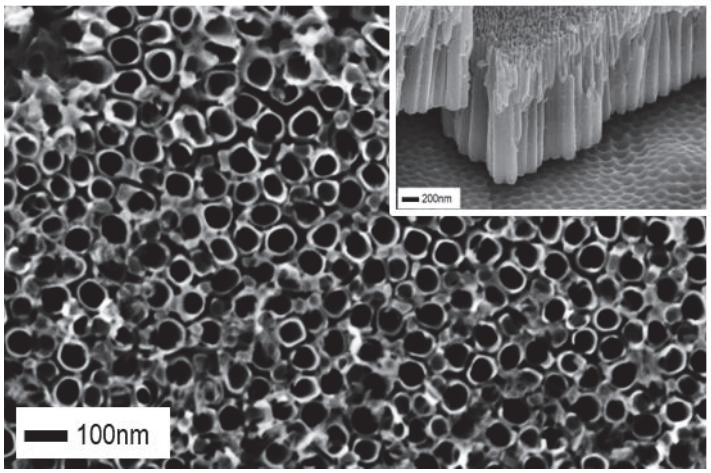

FIGURE 2. FE-SEM images. Top view of the Short NTs achieved following the anodization method AM6 in Tab.1 (6 %v/v H_2O). The insert (on top right) is the cross-sectional view.

Further increases in water content to > 6 %v/v (Tab.1, AM3-AM4) enhance the disorder of the nanostructure (Fig.3, A-B), while higher cell voltage growth rate (Tab.1, AM5) did not allow to attain the dissolution of the tree-like layer (Fig.3-C).

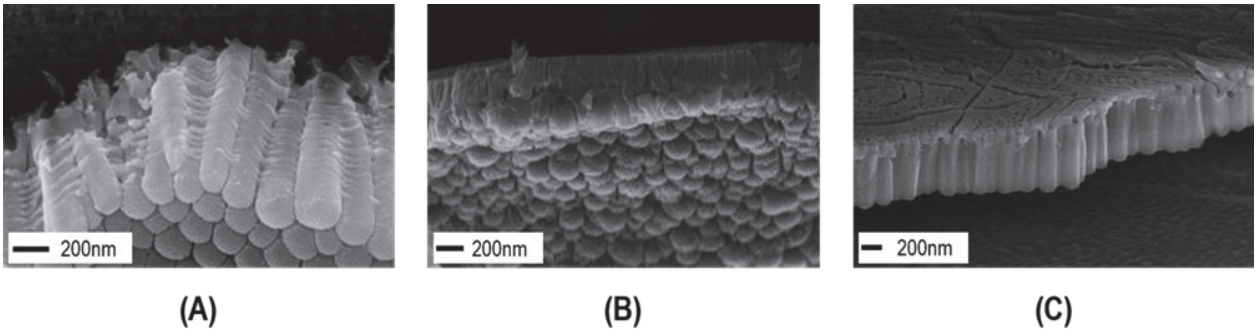

FIGURE 3. FE-SEM images, cross sectional views. A) 10% v/v H_2O (Tab.1, AM3); B) 15% v/v H_2O (Tab.1, AM3) and C) 6% v/v H_2O (Tab.1, AM5).

TiO_2 NTs synthesized with the anodization method AM1 and AM6 will be referred hereafter as Long and Short respectively.

TiO_2 Based Electrodes as Anodic Materials for Lithium-ion cells

In Fig.4-A and B are shown the lithium-ion insertion/extraction properties respectively of Short c-TiO_2 and Short a-TiO_2 NTs based electrodes. For all the investigated current densities c-TiO_2 shows well defined plateau at around 1.75 V (discharge cycles) and 2 V (charge cycles). It is related to the phase transition from lithium-poor anatase to lithium-rich titanate [3,20]. On the contrary, the sloping profile observed for a-TiO_2 highlights the pseudocapacitive behavior induced by surface defects and structural disorder, typical of electrodic materials with low crystallinity [4]. These differences are in good agreement with the XRD findings in Fig.5.

Although the capacity is not so high if compared to the theoretical value (335 mAh g^{-1}), the charge/discharge curves highlight good stability (i.e. specific capacitance reversibility) of both anodes tested (Fig.4-A and B).

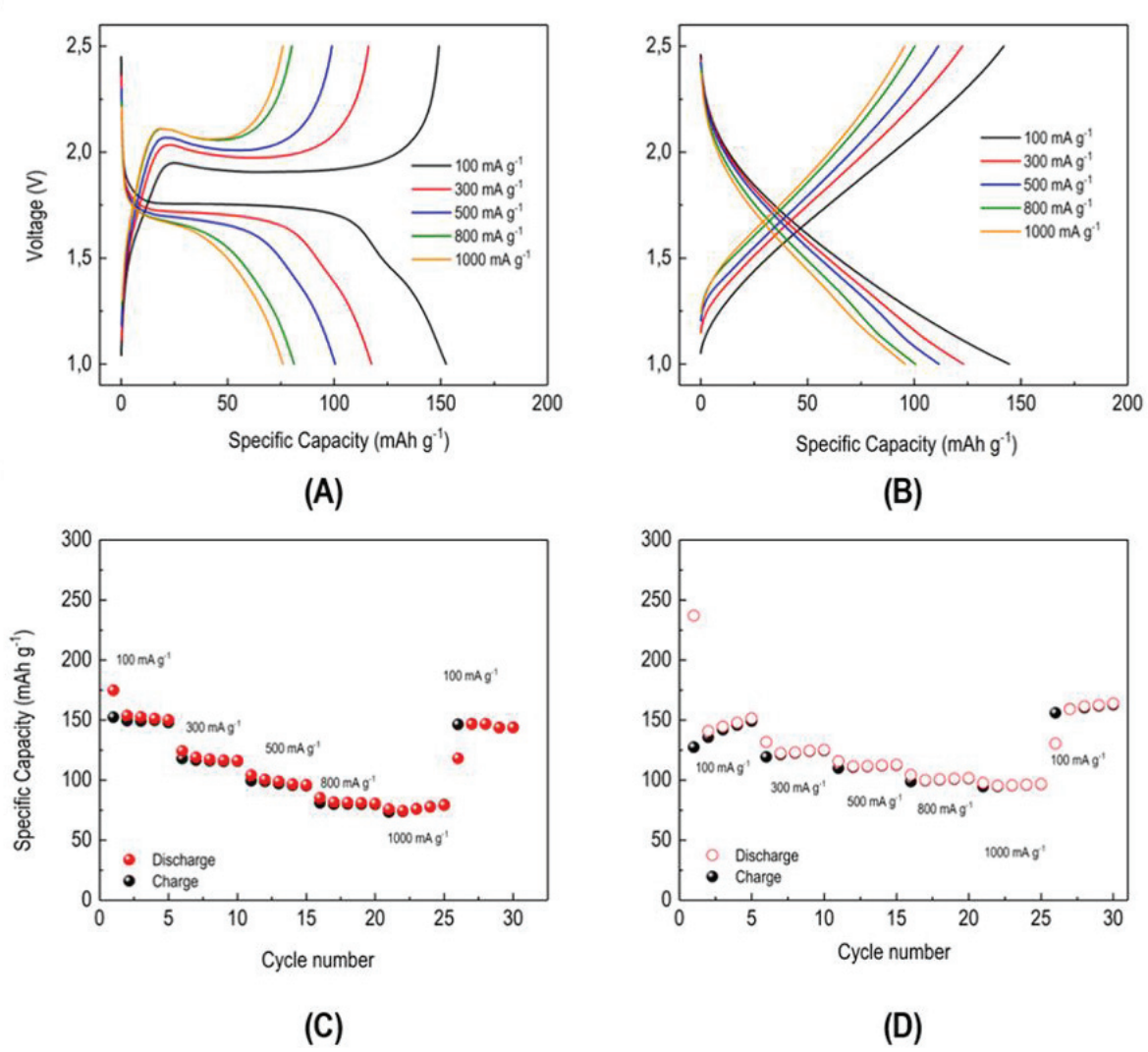

FIGURE 4. A, B) Galvanostatic discharge (lithium insertion)/charge (lithium extraction) curves (Vs Li^+/Li). C, D) Rate performances at different cycles. Short c-TiO_2 NTs (A and C) and Short a-TiO_2 NTs (B and D).

In Fig.4-C and D are shown the rate performances achieved in the same voltage windows and varying the number of cycles and the charge/discharge rates. Here, the trend just observed in the voltage/capacity curves comparing the two electrodes is confirmed. At 1000 mA g^{-1}, a-TiO_2 exhibits higher capacity compared to the c-TiO_2 based electrode. In the first discharge cycle, a-TiO_2 showed a capacitance of 236 mAh g^{-1} decayed at around 150 mAh g^{-1} in the second cycle. This irreversible capacity could be attributed to the solid electrode/electrolyte interface formation [21]. Furthermore, it is worth noting that in the last cycles, recorded at 100 mA g^{-1}, an increase in the capacity has been observed respect to first cycles (except for the first one) at the same rate, up to 160 mAh g^{-1}. It hasn't been the same for c-TiO_2 which showed comparable capacities.

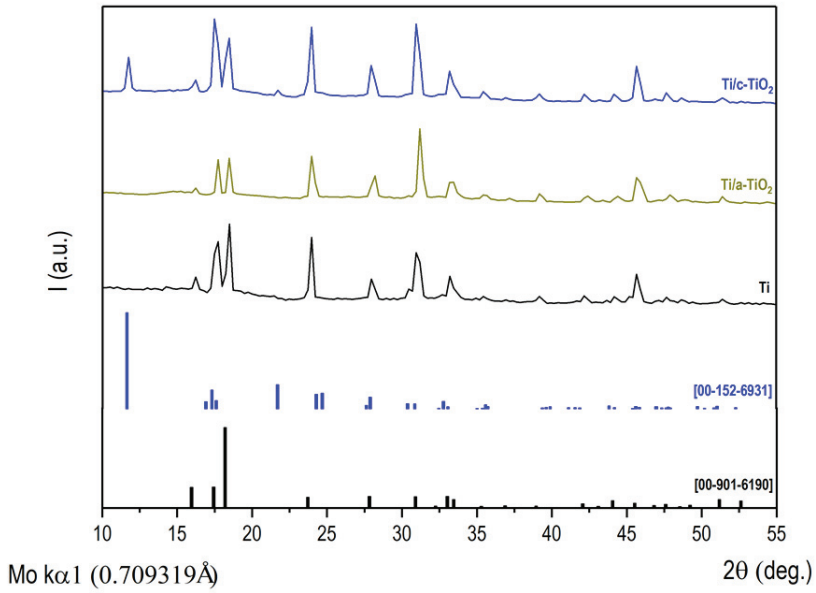

FIGURE 5. XRD characterization. The bars at the bottom are database reference patterns representative of Ti (black bars) and Anatase TiO_2 (blue bars). On the top are reported the experimental patterns collected for Ti (black line), a-TiO_2 based electrodes (dark yellow line) and c-TiO_2 based (blue line).

Based on these evidences, the last set of tests were carried out employing only the Long a-TiO_2 (Fig.6). As highlighted above for the Short a-TiO_2, the behavior of the voltage/capacity curves (Fig.6-A) achieved employing Long a-TiO_2 do not show plateau at any potential. Only at 100 mA g^{-1}, during the charge cycle a variation in the slope of the curve has been observed. In comparison to the Short a-TiO_2 at each current density higher capacity has been observed.

In Fig.6-B are shown the rate performances varying the number of cycles and the current densities. During the first discharge cycle a capacitance of ~400 mAh g^{-1} was recorded, higher than the theoretical value. Also in this case, the decay in sequent cycles at ~200 mAh g^{-1} is attributable to the solid electrode/electrolyte interface formation [21]. Remarkably, in the last cycles an increase in the capacity has been observed up to ~300 mAh g^{-1}, significantly higher than that observed for the Short a-TiO_2 in Fig.4-D.

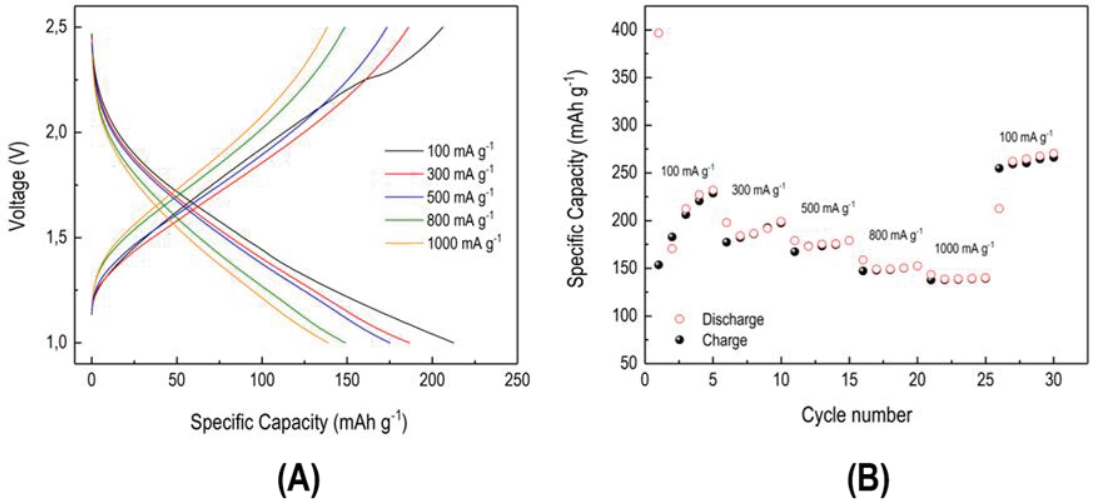

FIGURE 6. Long a-TiO_2 NTs. A) Galvanostatic discharge (lithium insertion)/charge (lithium extraction) curves (Vs Li^+/Li); and B) Rate performances at different cycles.

Further galvanostatic cycling, at 1000 mA g^{-1}, have been performed during prolonged cycling tests in order to evaluate the capacity retention of the electrodes. Figure 7 displays the specific capacity values during cycling for all the previously tested electrodes.

Long c-TiO_2 (~80 cycles) shows the highest specific capacitance and, remarkably, all the electrodes tested showed the same capacity proceedings with the number of cycles demonstrating an excellent capacity retention.

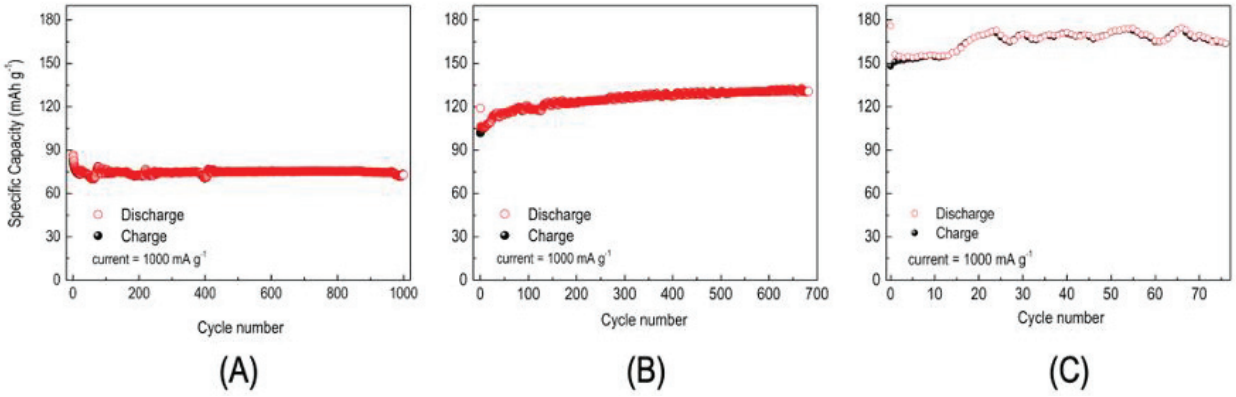

FIGURE 7. Rate performances at different number of cycles for: A) Short c-TiO_2; B) Short a-TiO_2 and C) Long a-TiO_2.

CONCLUSIONS

The optimization of the us developed single-step anodization method allowed to achieve electrodes characterized by different surface to volume ratios. Specifically, have been achieved two different NTs lengths by the adjustment of the electrolyte composition and the cell voltage growth rate during the potentiodynamic step at the early stage of the anodization.

The synthesized electrodes have been employed as anodes for LIBs. Here, a-TiO_2 exhibited the best performances in comparison to c-TiO_2. Furthermore, Long a-TiO_2 showed reversible capacitance at 100 mA g^{-1} close to the theoretical value. This last finding would suggest a further optimization study of the us developed NTs synthesis method which could be useful to fine control the lithium-ion insertion/extraction properties.

REFERENCES

1. W. Zhang, Y. Gong, N.P. Mellott, D. Liu, and J. Li, J. Power Sources **276**, 39 (2015).
2. L. Kavan, J. Solid State Electrochem. **18**, 2297 (2014).
3. V. Subramanian, A. Karki, K.I. Gnanasekar, F.P. Eddy, and B. Rambabu, J. Power Sources **159**, 186 (2006).
4. S. Li, P. Xue, C. Lai, J. Qiu, M. Ling, and S. Zhang, Electrochim. Acta **180**, 112 (2015).
5. J.M. Macák, H. Tsuchiya, and P. Schmuki, Angew. Chemie Int. Ed. **44**, 2100 (2005).
6. P. Roy, S. Berger, and P. Schmuki, Angew. Chemie - Int. Ed. **50**, 2904 (2011).
7. D. Regonini, C.R. Bowen, R. Stevens, D. Allsopp, and A. Jaroenworaluck, in *Phys. Status Solidi Appl. Mater. Sci.* (2007), pp. 1814–1819.
8. S.P. Albu and P. Schmuki, Phys. Status Solidi - Rapid Res. Lett. **4**, 215 (2010).
9. J.M. Macak, H. Tsuchiya, A. Ghicov, K. Yasuda, R. Hahn, S. Bauer, and P. Schmuki, Curr. Opin. Solid State Mater. Sci. **11**, 3 (2007).
10. A. Ghicov, H. Tsuchiya, J.M. MacAk, and P. Schmuki, Electrochem. Commun. **7**, 505 (2005).
11. K.S. Raja, T. Gandhi, and M. Misra, Electrochem. Commun. **9**, 1069 (2007).
12. C. Dumitriu, C. Pirvu, and I. Demetrescu, J. Electrochem. Soc. **160**, G55 (2012).
13. C.A. Grimes and G.K. Mor, *TiO2 Nanotube Arrays: Synthesis, Properties, and Applications* (2009).
14. A. Auer and J. Kunze-Liebhäuser, Small Methods **1800385**, 1800385 (2018).

15. L. -k. Tsui and G. Zangari, J. Electrochem. Soc. **161**, D3066 (2014).
16. N. Mir, K. Lee, I. Paramasivam, and P. Schmuki, Chem. - A Eur. J. **18**, 11862 (2012).
17. L.K. Tsui, T. Homma, and G. Zangari, J. Phys. Chem. C **117**, 6979 (2013).
18. M.M. Momeni and Y. Ghayeb, J. Alloys Compd. **637**, 393 (2015).
19. A. Rubino, P.G. Schiavi, P. Altimari, and F. Pagnanelli, in *AIP Conf. Proc.* (2019), p. 020005.
20. D. Bresser, B. Oschmann, M.N. Tahir, F. Mueller, I. Lieberwirth, W. Tremel, R. Zentel, and S. Passerini, J. Electrochem. Soc. **162**, A3013 (2015).
21. M. Pfanzelt, P. Kubiak, M. Fleischhammer, and M. Wohlfahrt-Mehrens, J. Power Sources **196**, 6815 (2011).